Eur J Nucl Med Mol Imaging (2009) 36:182–193
DOI 10.1007/s00259-008-0943-6

ORIGINAL ARTICLE

Assessment of various strategies for ^{18}F-FET PET-guided delineation of target volumes in high-grade glioma patients

Hansjörg Vees · Srinivasan Senthamizhchelvan · Raymond Miralbell · Damien C. Weber · Osman Ratib · Habib Zaidi

Received: 6 July 2008 / Accepted: 9 August 2008 / Published online: 26 September 2008

Abstract
Purpose The purpose of the study is to assess the contribution of ^{18}F-fluoro-ethyl-tyrosine (^{18}F-FET) positron emission tomography (PET) in the delineation of gross tumor volume (GTV) in patients with high-grade gliomas compared with magnetic resonance imaging (MRI) alone.
Materials and methods The study population consisted of 18 patients with high-grade gliomas. Seven image segmentation techniques were used to delineate ^{18}F-FET PET GTVs, and the results were compared to the manual MRI-derived GTV (GTV_{MRI}). PET image segmentation techniques included manual delineation of contours (GTV_{man}), a 2.5 standardized uptake value (SUV) cutoff ($GTV_{2.5}$), a fixed threshold of 40% and 50% of the maximum signal intensity ($GTV_{40\%}$ and $GTV_{50\%}$), signal-to-background ratio (SBR)-based adaptive thresholding (GTV_{SBR}), gradient find (GTV_{GF}), and region growing (GTV_{RG}). Overlap analysis was also conducted to assess geographic mismatch between the GTVs delineated using the different techniques.
Results Contours defined using $GTV_{2.5}$ failed to provide successful delineation technically in three patients (18% of cases) as $SUV_{max}<2.5$ and clinically in 14 patients (78% of cases). Overall, the majority of GTVs defined on PET-based techniques were usually smaller than GTV_{MRI} (67% of cases). Yet, PET detected frequently tumors that are not visible on MRI and added substantially tumor extension outside the GTV_{MRI} in six patients (33% of cases).
Conclusions The selection of the most appropriate ^{18}F-FET PET-based segmentation algorithm is crucial, since it impacts both the volume and shape of the resulting GTV. The 2.5 SUV isocontour and GF segmentation techniques performed poorly and should not be used for GTV delineation. With adequate setting, the SBR-based PET technique may add considerably to conventional MRI-guided GTV delineation.

Keywords PET/CT · ^{18}F-FET · Image segmentation · Gross tumor volume · High-grade glioma

Introduction

The standard treatment of high-grade glioma consists of surgery and radiation therapy (RT) with concomitant and adjuvant chemotherapy [1]. Unfortunately, the demonstrated benefit of RT does not extend to cure for the vast majority of patients. As RT is the backbone of the treatment strategy, defining the precise gross tumor volume (GTV) is of paramount importance. For the diagnosis of primary brain tumors, magnetic resonance imaging (MRI) and computed tomography (CT) are the imaging modalities of choice [2, 3]. As such, these are also used in the postoperative setting for GTV delineation [4]. However, a real measure of tumor extension in high-grade gliomas is quite difficult with either modality. In the particular case of recurrent gliomas, MRI was found to have a low specificity to distinguish between side effects of therapy and tumor recurrence corresponding to only 50–53% [5, 6].

H. Vees · S. Senthamizhchelvan · O. Ratib · H. Zaidi
Service of Nuclear Medicine, Geneva University Hospital, CH-1211, Geneva, Switzerland

H. Vees · R. Miralbell · D. C. Weber
Service of Radiation Oncology, Geneva University Hospital, CH-1211, Geneva, Switzerland

H. Zaidi (✉)
Division of Nuclear Medicine, Geneva University Hospital, CH-1211, Geneva 4, Switzerland
e-mail: habib.zaidi@hcuge.ch

Recently, positron emission imaging (PET) was recognized as a valuable tool in the primary and secondary diagnosis of high-grade gliomas [3]. ^{18}F-fluoro-deoxy-glucose (FDG) as probe is not very useful in the diagnosis of brain tumors, since the normal brain has a high metabolic activity and thus does not allow differentiating between normal cerebral tissue and tumors [7]. Radiolabeled amino acids can pass the blood–brain barrier independently of its disturbance. A variety of ^{11}C- and ^{18}F-labeled amino acids such as ^{11}C-methionine (^{11}C-MET) and ^{18}F-fluoro-ethyl-tyrosine (^{18}F-FET) have been studied for potential use in oncologic PET [8]. Most brain tumors show an increased uptake of amino acids compared with normal brain. In particular, the uptake of ^{18}F-FET by brain tumors especially by high-grade glioma cells is intense relative to the low uptake in normal cerebral tissue [9]. ^{18}F-FET PET showed its potential in the detection of primary and recurrent brain tumors with high sensitivity and specificity [5, 10–13].

One of the most difficult issues facing PET-based radiation therapy treatment planning is the accurate delineation of target regions from typical noisy functional images [14]. The major problems encountered in functional volume quantitation are image segmentation and imperfect system response function. Image segmentation is defined as the process of classifying the voxels of an image into a set of distinct classes. The difficulty in image segmentation is compounded by the low spatial resolution and high noise characteristics of PET images. Medical image segmentation has been identified as the key problem of medical image analysis and remains a popular and challenging area of research. Despite the difficulties and known limitations, several image segmentation approaches have been proposed and used in clinical setting. These include thresholding, region growing, classifiers, clustering, edge detection, Markov random field models, artificial neural networks, deformable models, atlas-guided, and many other approaches [15, 16].

At present, various methods are used in practice to delineate PET-based target volumes [16–25]. The manual delineation of target volumes using different window level settings and look up tables is the most common and widely used technique in the clinic. However, the method is highly operator-dependent and is subject to high variability between operators [20, 26]. Semiautomated or fully automated delineation techniques might offer several advantages over manual techniques by reducing operator error/subjectivity, thereby improving reproducibility. However, despite the remarkable progress that automated image segmentation has made during the last few years, performance validation in a clinical setting remains the most challenging issue [27]. When using clinical data where the ground truth is not known a priori, it is generally unacceptable to use an imaging modality as gold standard against which results from another imaging modality are compared. Therefore, the objective of this study is to compare GTVs delineated using structural MRI with those obtained using various strategies for ^{18}F-FET PET-based image segmentation techniques for high-grade gliomas in the absence of a gold standard providing the independent truth.

Material and methods

Patients

This prospective study was approved by the institutional ethical committee. A signed informed consent was obtained from all patients participating in the study protocol. The 20 patients were refereed to the Division of Nuclear Medicine of Geneva University Hospital between July 2006 and December 2007. The mean age of the patients was 54 years. The clinical characteristics and referral patterns of the patient population are summarized in Table 1. Given that ^{18}F-FET tracer is not registered in Switzerland, it was administered under the ruling of "compassionate use", which requires approval on a patient by patient basis by the Swiss federal authorities (Swissmedic and the Federal Office of Public Health). Two patients (one with brainstem tumor and one with anaplastic astrocytoma) were excluded due to technical problems. The remaining 18 patients had histologically proven high-grade gliomas (grade III, 4 patients; grade IV, 14 patients). The inclusion criteria for the trial were the diagnosis of inoperable high-grade glioma

Table 1 Clinical characteristics and referral patterns of the patient population included in the study protocol (n=18)

Characteristics	Number (%)
Age (year)	
Mean 54, range 20–75	
Sex	
Men	8 (44)
Women	10 (56)
Karnofsky performance status	
100	4 (22)
90	3 (17)
80	7 (39)
70	4 (22)
Histologic characteristics	
Glioblastoma WHO IV	14 (77)
Astrocytoma WHO III	2 (11)
Oligodendroglioma WHO III	1 (6)
Oligoastrocytoma WHO III	1 (6)
Indication for PET/CT	
Recurrence	1 (6)
After partial resection	9 (50)
After biopsy in unresectable tumor	8 (44)

or the suspicion of residual tumor on structural MRI performed during the first 24 h postoperatively and/or the intraoperative diagnosis of possible residual tumor. In eight patients, PET scanning was performed after partial resection of the high-grade glioma (median time 13 days) and in nine patients after biopsy of inoperable high-grade glioma (median time 16.5 days). One patient presented with a recurrent anaplastic astrocytoma grade III, 4 years after partial resection and intermittent chemotherapy with Temozolomide. The recurrence was histologically proven by biopsy.

^{18}F-fluoro-ethyl-tyrosine

^{18}F-fluoro-ethyl-tyrosine was prepared according to good manufacturing practice standards at the Centre of Radiopharmacy, University Hospital of Zurich, Switzerland and delivered to our department. All patients were injected a standard activity of 200 MBq ^{18}F-FET, which resulted in an average effective dose of 3.3 mSv [28].

PET/CT scanning

All patients had a diagnostic quality PET/CT scan of the brain in radiotherapy treatment position on a dedicated combined scanner equipped with a set of three triangulation lasers (central and laterals) similar to those used for standard CT-based virtual simulation. For CT scanning, contrast enhancement was not used in this particular population. Patient positioning was verified by individual plastic masks. The simulation was carried out by experienced radiation therapy technologists trained specially for this purpose. PET imaging of the brain and non-enhanced CT with 2-mm slice thickness were acquired in all patients using a Biograph 16 PET/CT scanner (Siemens Medical Solutions, Erlangen, Germany) operating in 3D mode. Patients were placed in scanning position and CT imaging performed under standard conditions using 120 kVp, 90 mAs, 16×1.5 collimation, a pitch of 0.8 and 0.5 s/rotation. Patients were injected intravenously after 4–6h fasting periods. Listmode PET data acquisition started immediately following tracer injection for a total duration of 30 min to allow a flexible choice of reconstruction frames. The dynamic study corresponds to a single bed position covering the head up to the second cervical vertebral body. An additional late static acquisition (10 min) in the same position was also performed after the listmode study in 12 patients.

Dynamic series of 3×10 min were reconstructed using the standard clinical protocol recommended by the manufacturer to define the sequence showing the highest uptake in the brain tumors compared to the normal brain tissue. Following Fourier rebinning and model-based scatter correction, PET images were reconstructed using two-dimensional iterative normalized attenuation-weighted ordered subsets expectation maximization (NAW-OSEM). The CT-based attenuation correction map was used to reconstruct the emission data. The default parameters used were OSEM iterative reconstruction width four iterations and eight subsets followed by a post-processing Gaussian filter (kernel full-with half-maximal height, 5 mm).

The PET, CT, and fused PET/CT images were displayed for review in axial, coronal, and sagittal planes. All studies were interpreted and reviewed with knowledge of the patient's clinical history and results of previous imaging studies. A team involving two experienced nuclear medicine physicians and an experienced radiologist interpreted the ^{18}F-FET PET/CT images. A multimodality computer platform (Syngo Multimodality Workplace, Siemens Medical Solutions, Erlangen, Germany) was used for image review and interpretation. A site of increased ^{18}F-FET uptake was defined as benign and unrelated to cancer when it is located in an area corresponding to the physiologic biodistribution of the tracer or when related to known nonmalignant physiologic process. A focus of increased ^{18}F-FET uptake, with intensity higher than that of surrounding tissues, in areas unrelated to physiologic or benign processes, was defined as malignant. All PET studies showing at least one site of abnormal ^{18}F-FET uptake characterized as malignant were defined as positive. The maximum standardized uptake value (SUV_{max}) was calculated for regions of interest (ROIs) of focal hyperactivity by dividing the observed activity concentration in attenuation-corrected PET data with the injected activity per gram body weight. The SUV_{max} of each lesion was calculated for the corresponding dynamic time frame considered by applying appropriate decay correction.

Magnetic resonance imaging

High-resolution gadolinium-enhanced three-dimensional MR brain images were obtained for all clinical studies, except one patient. This patient presented a contraindication for MRI owing to the presence of two intracranial metallic bullets. The MRI was practiced at a mean of 16.9 days (range 7 to 35) before the PET/CT study. All patients undergoing a partial resection had a postoperative MRI during the first 24 h following surgery.

The MRI was performed either on a 1.5-T Gyroscan Intera MRI scanner (Philips Medical systems, Cleveland, OH, USA) or a 3-T Magnetom Trio MRI scanner (Siemens Medical Solutions, Forchheim, Germany) equipped with a standard head coil. The MRI protocol consisted of a T1-weighted sequence (25 cm axial field of view, 7.8 s repetition time, 256×256 matrix size, 160 axial slices with 1.1 mm slice thickness both before and 2 min. after injection of 0.2 ml/kg gadolinium). A sagittal and coronal

fluid attenuation inversion recovery (FLAIR) as well as a T2-weighted axial sequence were also performed with a slice thickness of 5 mm for each sequence. In addition, MR spectroscopy was performed on the side corresponding to the brain tumor and on the contralateral side.

Phantom experiment for derivation of the SBR algorithm

In diagnostic and oncological PET imaging, if the intention is to measure the volume and uptake in a specific lesion, it is convenient to make preliminary phantom studies on an object of similar shape and size with the assumption that the size, shape, location, density, and intensity of the simulated object and surrounding tissues are comparable to that of the patient to be measured. The SBR technique requires calibration data that are applicable for quantification of tumor volumes in clinical oncology. The NEMA IEC/2001 image quality body phantom (Fig. 1A,B) consisting of an elliptical water-filled cavity with six spherical inserts suspended by plastic rods of volumes 0.5, 1.2, 2.6, 5.6, 11.5, and 26.5 cc (inner diameters of 1.0, 1.3, 1.7, 2.2, 2.8, and 3.7 cm) was used to derive the parameters required for implementation of the adaptive thresholding algorithm based on SBR estimates. The spheres were filled with ^{18}F activity concentration ranging from 20 to 47 kBq/cc. The water cavity was first filled with increasing activity of ^{18}F to get SBRs of 10.0, 8.6, 6.9, 5.0, 3.3, and 2.1. These activity ratios were chosen to simulate the range of SBRs observed in clinical conditions. For all SBR ratios, 15 min PET data acquisitions were performed on the same Biograph PET/CT scanner used for patient studies (Siemens Medical Solution, Erlangen, Germany). The images were reconstructed using the same processing protocol applied to clinical studies. The SBRs were measured from all combinations of spheres and background activity concentrations. The maximal activity of the spheres was defined as the average activity of the eight voxels surrounding the hottest voxel. The background activity concentration was measured in planes containing the spheres using eight circular ROIs with a diameter of 5 cm, where the mean value of all ROIs was considered as background activity concentration. The diameter and volume of each sphere was successively calculated using increasing thresholds, where the thresholds were determined as a percentage of the maximal activity in the spheres. The optimal thresholds which resulted in minimal least square difference between measured and actual sphere volumes were obtained (Fig. 2C). The smallest sphere of 0.5 cc with a diameter of 10 mm was excluded from the analysis to avoid the significant bias of partial volume effect owing to the limited spatial resolution of the scanner. The measured SBR and the resultant threshold were fitted using an inverse function (Threshold $= a + b \times 1/\mathrm{SBR}$) to yield the best regression parameters for the equation which allows estimation of the optimal threshold independent of any a priori knowledge of the lesion characteristics and tumor location. The results were almost similar when the SBR measurements were performed in a head-sized phantom thus confirming the applicability of the technique for almost all tumor locations.

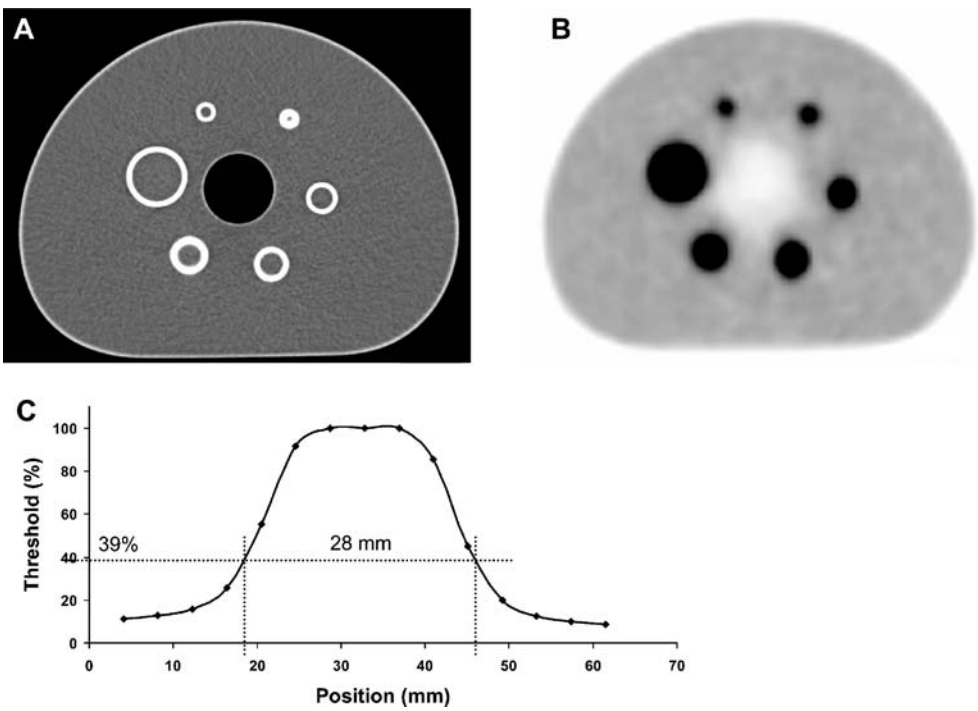

Fig. 1 (**A**) Computed Tomography (CT) and (**B**) corresponding PET transaxial slices of the whole-body NEMA IEC/2001 image quality body phantom used to derive the parameters required for implementation of the adaptive thresholding algorithm. The phantom consists of an elliptical water filled cavity with six spherical inserts suspended by plastic rods, of inner diameters of 1.0, 1.3, 1.7, 2.2, 2.8, and 3.7 cm. A horizontal profile through the sphere having a diameter of 2.8 cm illustrating the signal-to-background ratio (SBR)-specific threshold (39%) that best corresponded to the physical diameter of the spherical source is also shown (**C**)

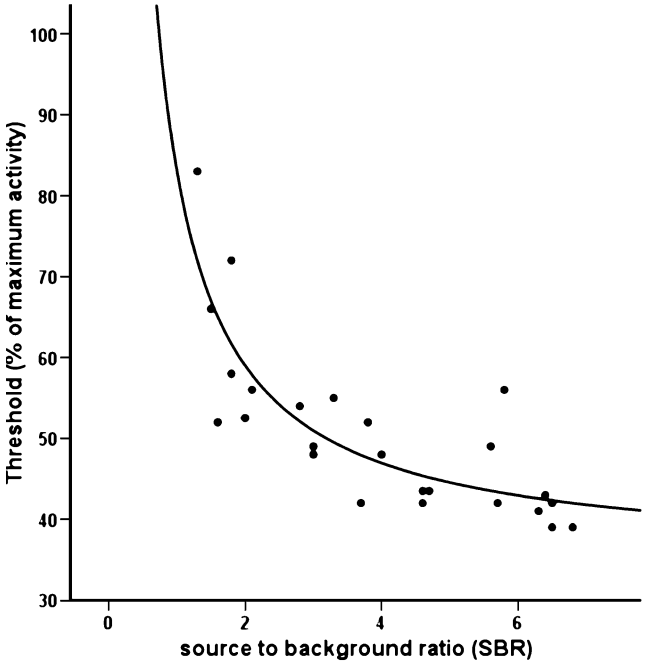

Fig. 2 Plots of the relationship between the signal-to-background ratio and the threshold to be applied to fit spheres of volumes ranging between 1.2 and 26.5 cc. The data were fitted using an inverse function of the form Threshold $= a + b \times 1/$ SBR

Gross tumor volume delineation

Manual GTV delineation

The brain MR images were first coregistered to their respective PET/CT images using an automated image registration software embedded within the TrueD software (Siemens Medical Solutions, Erlangen, Germany). A linear rigid-body registration using a traditional nine-parameter model was used. The same software was also used for manual delineation of the GTV. The conventional MRI-based GTV (GTV_{MRI}) and the PET-based GTV (GTV_{man}) were delineated manually in two separate sessions by an experienced radiation oncologist. For GTV_{MRI} delineation, a gadolinium-enhanced T1-weighted gradient-echo sequence was used. The image matrix consisted of 256×256×160 voxels, with a resolution in the transaxial direction of 0.97×0.97 mm^2 and an axial resolution of 1.1 mm. Besides the information from the dynamic PET series, all clinical history and previous imaging studies including complementary MRI sequences were provided. In a second session, the same radiation oncologist delineated the GTV_{man} consensually using appropriate window-level settings for identifying the tumor from background. Clinical interpretation as well as GTV_{man} delineation was performed on static images reconstructed from the listmode data in the interval between 10 and 20 min which proved to be the sequence resulting in the highest contrast between the tumors and normal brain tissue.

Semiautomated PET image segmentation techniques

Six semiautomated image segmentation techniques were used to obtain PET-derived GTVs. The GTVs were delineated using the *RT_Image* software [29]. An isocontour of SUV 2.5 around the tumor region was used to obtain an SUV threshold-based cutoff GTV ($GTV_{2.5}$). In addition, a fixed threshold of 40% and 50% of the maximum signal intensity was also used to delineate $GTV_{40\%}$ and $GTV_{50\%}$, respectively. The GTV delineation based on region growing (GTV_{RG}) and gradient find (GTV_{GF}) segmentation algorithms were obtained using techniques described in the aforementioned reference [29].

Region growing approaches exploit the fact that voxels which are close to each other have comparable gray values. Region growing is a bottom–up procedure starting with a set of seed pixels and growing to a homogeneous connected region from each seed. The user usually selects a voxel, and a region grows out from that seed until some criteria for stopping growth are met. Briefly, the RG technique used in this work finds the voxel of maximum intensity from the seed along the projection line. The segmented region consists of all voxels connected to the local voxel containing maximum intensity within a 10-mm diameter sphere that have an intensity greater than 50% of the local maximum intensity. On the other hand, edge detection-based approaches exploit the existence of abrupt changes in gray level intensity values to delineate edges that are formed at the intersection of two regions. Edge detection techniques work relatively well on images with good contrast between regions. An edge is marked if a significant spatial change occurs in the second derivative. For the GF algorithm, segmentation is performed on a region identified as pathologic through user interaction. This region is generated following appropriate seed selection to initiate the above described RG technique. The algorithm used is a variant of the Marr–Hildreth edge detector that iteratively adjusts the contours toward a zero crossing in the second gradient, which corresponds to a local maximum of the gradient magnitude. Finally, the popular signal-to-background ratio (SBR)-based adaptive thresholding technique described in [18] was used to obtain GTV_{SBR}. The scanner-specific parameters required for derivation of the adaptive threshold calibration curve was obtained through a phantom experiment with various signal to background ratios as described in the phantom experiment section above. For GTV_{SBR} delineation, the maximum signal intensity of the tumor was defined as the mean activity of the hottest voxel and its eight surrounding voxels in a transversal slice, whereas the mean background activity

was obtained from a manually drawn ROI far away from the tumor.

Tumor delineation was considered unsuccessful if the resulting volume contained only small parts of the tumor, substantially large parts of visually normal tissue (as observed on GTV_{SBR} and GTV_{man}), or because of technical impossibility of the contouring (e.g., $SUV_{max} < 2.5$ makes it impossible to draw a $GTV_{2.5}$). The GTVs obtained by using semiautomated delineation algorithms were checked visually by an experienced radiation oncologist before approval.

Statistical analysis of GTVs

To assess geographic mismatch between the GTVs delineated using the different segmentation techniques, the following overlap analysis were performed: (1) The overlap volume of GTV_{MRI} and GTV_{PET}, for which overlap was expressed as the overlap volume of GTV_{MRI} and GTV_{PET} relative to GTV_{MRI}–overlap fraction (OF) MRI [OF_{MRI}]; (2) the overlap volume of GTV_{MRI} and GTV_{PET} relative to the PET-based GTVs–overlap fraction PET [OF_{PET}]; (3) the volume enclosed by GTV_{MRI} but not by GTV_{PET} relative to GTV_{MRI}, which is $1-OF_{MRI}$; and (4) the volume enclosed by GTV_{PET}, but not by GTV_{MRI} relative to GTV_{PET}, which is $1-OF_{PET}$. In addition, the overlap volume of GTV_{PET} and GTV_{SBR} relative to GTV_{SBR} was also calculated. Statistical analyses and curve fitting were performed using SPSS® (version 15.0, SPSS, Chicago, IL, USA). Regression analyses were used to evaluate difference between calculated volumes and overlap between GTVs when using the different segmentation tools. The level of statistical significance adopted was 0.05.

Results

Figure 2 shows plots of the threshold to be applied to fit spheres of volumes ranging between 1.2 and 26.5 cc vs. the SBR. The regression parameters of the inverse function ($\text{Threshold} = a + b \times 1/\text{SBR}$) that best fitted the experimental results are a=34.9 and b=48.2. Consistent with the observations made by previous investigators [18, 30], this relationship indicates that a higher threshold is required to accurately estimate the actual volume of objects with low contrast (i.e., low SBR). To avoid the slight dependence of the threshold required to adequately measure the actual volume of the spheres and thus the derived regression parameters on image reconstruction technique and selected parameters, the same reconstruction algorithm and associated parameters (number of iterations, subsets, and post-reconstruction smoothing) used in clinical studies were applied.

PET detected frequently tumors that are not visible on MRI and added substantially tumor extension outside the GTV_{MRI} in six patients (33% of cases). Figure 3 shows one such example where tumors were only detected on the ^{18}F-FET PET study and completely missed on MRI. The comparison of GTV delineation based on MRI and seven ^{18}F-FET PET-based GTVs is summarized in Table 2. In all 18 patients, MRI images could identify 19 lesions, whereas FET PET images identified 24 lesions, i.e., the ^{18}F-FET PET images could identify five lesions which were not seen on MRI. Out of the seven ^{18}F-FET PET GTV segmentation techniques only $GTV_{2.5}$ and GTV_{GF} was not successful in four of 24 and in eight of 24 lesions delineation, respectively, due to technical difficulties. Overall, the GTVs delineated by 2.5 SUV isocountour ($SUV_{2.5}$) and GF were neither realistic nor comparable with other segmentation techniques in most of the lesions, even though they were technically feasible. The failure of GF technique in delineating realistic GTV could be due to low and inhomogeneous tumor uptake. Hence for the sake of comparison of GTV delineation between MRI and other FET PET-based techniques, the $SUV_{2.5}$ and GF techniques were excluded from further analysis.

Figure 4 shows a typical example of a patient study presenting with a glioblastoma illustrating differences in target-volume definition obtained using the various methods described above compared to GTV_{MRI}. For this particular patient (patient no. 7 in Table 2), all PET-based techniques define almost similar contours on this plane, but overall, the estimated lesion volume is different. Figure 5 illustrates 3-D volume rendering of the GTVs assessed using the various segmentation techniques and overlap analysis of the geographic match/mismatch between the defined GTVs. Indicated are GTV_{MRI} and three PET-based GTVs including GTV_{man}, GTV_{RG}, and GTV_{SBR}. Also shown are the overlaps between GTV_{MRI} and GTV_{man}, GTV_{RG}, and GTV_{SBR}, respectively. Note that for this particular tumor, GTV_{man} practically comprised approximately 95% of GTV_{MRI}. Figure 6 shows the comparison of mean absolute tumor volumes for 18 patients in only 19 lesions where MRI, manual delineation, thresholding using 40% and 50% of the maximum intensity, as well as RG and SBR techniques were able to adequately delineate the tumor volume (GF and SUV 2.5 were excluded in this analysis). Error bars indicate SD on the mean. Overall, none of the techniques yielded similar volumes relative to GTV_{MRI}.

The GTVs delineated using the different methods and OFs between various segmentation tools are summarized in Table 3. The mean volumes are for 18 patients, and only 19 lesions were similar to Fig. 6; the retained segmentation technique were only those that were able to adequately delineate the tumor volume (GF and $SUV_{2.5}$ were excluded

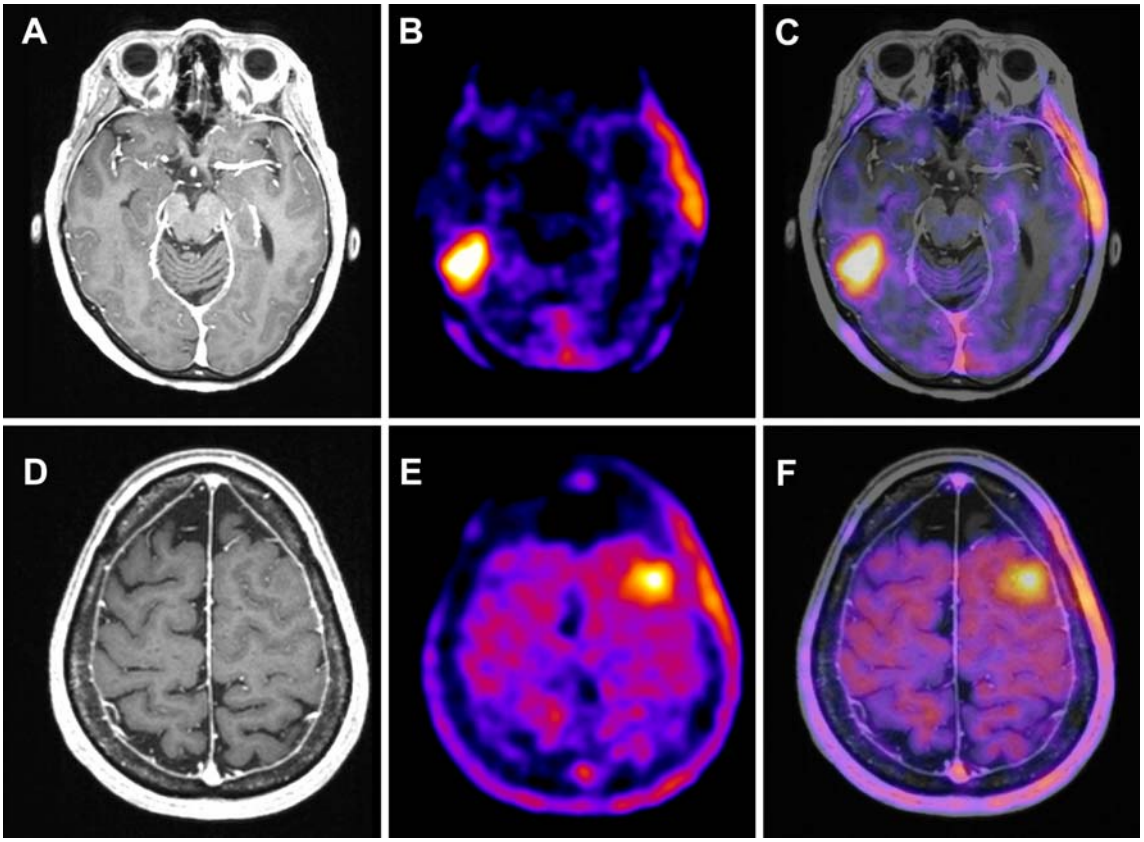

Fig. 3 Illustration of two clinical studies where tumors were only detected on the ^{18}F-FET PET study and missed on structural MRI. The images shown on the top row correspond to gadolinium enhanced T1-weighted MRI (**A**), coregistered PET (**B**) and fused PET/MR (**C**) of the first study. The same is shown in the *bottom row* for the second study (**D**, **E**, and **F**)

in this analysis). The mean OF_{MRI} varied from 0.14 to 0.54 depending on the segmentation technique used, whereas the mean OF_{PET} varied from 0.45 to 0.67. The mean GTV fraction was delineated by MRI, but not by PET (i.e., $1-OF_{MRI}$) varied between 0.46 and 0.86, whereas the mean GTV fraction was delineated by PET, but not by MRI ($1-OF_{PET}$), which varied between 0.33 and 0.55. The mean absolute volume, OF_{MRI}, and OF_{PET} for GTV_{man} vs. GTV_{SBR} and GTV_{RG} vs. $GTV_{50\%}$ were almost similar. OF_{SBR} is a comparison of OF within PET-defined volumes, which explains the lack of results for GTV_{MRI}. The *p* values are reported for OFs relative to OF_{SBR} as obtained by linear regression analysis.

Discussion

Among various functional imaging techniques, PET is considered the most powerful modality for providing an accurate, reliable, and reproducible estimate of various physiological and metabolic parameters [31]. Visual or qualitative assessment of PET images provides a relative and subjective impression regarding the overall landscape of function at the sites examined, particularly when the aim is to delineate target volumes in radiation treatment planning and to evaluate treatment response. For the former application, the most critical point is image segmentation, which is the process of identifying malignant lesions in the PET data and delineating their spatial occupation in the images. Image segmentation has been identified as the key problem of medical image analysis and remains a popular and challenging area of research. Manual and automated segmentation of patient image volumes for the purpose of quantifying tumor size, shape, and uptake has received significant attention during the last decade [15]. At present, different segmentation methods exist for PET-based target volume delineation. Among them, manual contouring by visual examination is the most commonly used method. The principal drawback of this method is that, it is highly subjective rather than objective due to various window-level settings used by different operators and varied perceptions of individuals owing to the inherent complexity of the human visual system. To limit intra- and inter-observer dependence and variability, the development of unsupervised segmentation algorithms is highly desired. The need for highly objective and automatic segmentation

Table 2 Summary of gross tumour volumes derived from MRI and estimated using the different PET image segmentation techniques

Pt. No	Histology	Tumour site	MRI Volume (cc)	^{18}F-FET PET Volume (cc)						
			GTV_{MRI}	GTV_{man}	GTV_{SBR}	GTV_{RG}	$GTV_{40\%}$	$GTV_{50\%}$	GTV_{GF}	$GTV_{2.5}$
1	AIII	Occipital	57.4	25.1	15.9	11.9	19.8	11.9	12.1	4.3
		Temporal	27.6	28.3	19.3	16.1	27.9	14.7	–	1.8
2	AIII	Thalamus	33.8	8.0	7.7	12.9	33.8	12.9	12.6	0.6
3	GBM	Parietal	–	9.7	7.4	6.1	9.8	5.8	5.4	5.6
		Frontal	20.9	12.6	6.0	4.9	9.3	4.7	4.4	4.1
		Frontal	–	4.4	5.5	3.6	11.7	4.2	3.2	0.3
4	GBM	Frontal	79.9	23.7	30.0	28.9	37.7	28.8	28.1	11.4
5	ODIII	Occipital	34.1	55.2	23.1	35.8	29.3	42.5	39.7	16.2
6	GBM	Frontal	–	22.9	21.5	20.5	44.2	19.6	–	2.4
		Parietal	19.0	10.6	8.4	7.6	13.6	7.8	7.2	3.6
7	GBM	Frontal	23.9	48.9	38.4	30.9	45.8	32.2	28.3	19.4
		Parietal	–	3.3	2.4	1.9	3.1	1.7	1.4	1.1
8	GBM	Temporal	65.4	60.8	42.7	31.8	50.8	31.8	31.2	26.2
9	OAIII	Frontal	34.0	25.9	33.1	18.2	89.4	16.8	–	0.3
10	GBM	Parietal	72.9	73.0	57.6	42.2	69.7	40.6	41.9	–
11	GBM	Frontal	76.9	42.2	53.1	61.9	57.8	26.4	–	7.8
12	GBM	Frontal	34.5	22.1	34.9	30.3	43.9	29.5	–	1.0
13	GBM	Frontal	23.5	32.4	24.7	22.0	28.6	23.9	22.6	7.0
14	GBM	Temporal	25.1	47.2	46.2	39.6	55.4	40.0	36.7	58.3
15	GBM	Temporal	13.4	4.9	29.0	8.3	35.3	5.8	–	–
16	GBM	Parietal	40.7	45.3	34.2	41.8	37.0	41.7	41.4	–
		Frontal	–	0.7	3.8	0.9	5.1	0.9	–	–
17	GBM	Frontal	41.8	12.0	11.0	6.0	10.4	5.9	5.4	2.0
18	GBM	Frontal	39.8	22.9	46.4	49.6	62.7	45.2	–	5.9

AIII Anaplastic astrocytoma WHO III, *OAIII* anaplastic oligoastrocytoma WHO III, *ODIII* anaplastic oligodendroglioma WHO III, *GBM* glioblastoma WHO IV

methods was largely recognized, and various groups have formulated different algorithms for image segmentation [16]. Segmentation by fixed thresholds of 40%, 50% of maximum intensity levels, isocontouring of $SUV_{2.5}$, adaptive thresholding using the signal to background ratio, region growing, clustering, gradient-based edge detection, and statistical Markov random field models are the most frequently used automatic procedures.

In this study, we compared seven PET-based techniques for delineation of GTV relative to MRI-guided derivation of GTV. Out of the seven ^{18}F-FET PET GTV segmentation techniques, only $GTV_{2.5}$ and GTV_{GF} were not successful in three of 18 and in eight of 18 patients, respectively, due to technical difficulties. The ^{18}F-FET PET-detected tumors were highly heterogeneous and had quite variable signal to background ratios. In most of the cases, the maximum tumor uptake was low compared to typical FDG studies; hence, the use of the empirical $SUV_{2.5}$ technique seems to be rather unrealistic as can be observed on the volumes delineated by this method which are grossly different from the remaining segmentation methods. Image segmentation using GF also does not seem to be relevant, as the tumor volumes had many signal minima and maxima combined with low-signal uptake making the technique not ideal for this group of patients.

From the overlap analysis, it was observed that OF_{MRI} decreased and OF_{PET} increased, from $GTV_{40\%}$ to GTV_{man} to GTV_{SBR}, GTV_{RG}, $GTV_{50\%}$ which implies that in this order, as the PET volume decreased, it was increasingly incorporated within the MRI volume. Though the mean absolute volumes, OF_{MRI}, and OF_{PET} of GTV_{man} vs. GTV_{SBR} and GTV_{RG} vs. $GTV_{50\%}$ were similar, when the analysis was done on an individual patient basis, the geographic mismatch was found to be substantial in many cases. The relatively small number of clinical studies included in this work is mainly due to financial constraints given that brain ^{18}F-FET PET is not a reimbursed indication in Switzerland. It should be emphasized, however, that the number is sufficient for reliable statistical analysis thus allowing reaching the objectives set.

Most other studies comparing GTV delineations in brain tumors using ^{18}F-FET [32–34] or ^{11}C-MET [35–38] against MRI reported that the addition of PET information modified significantly the shape and the extension of the GTV. The SBR-based method for GTV delineation is arguably the only automatic PET image segmentation

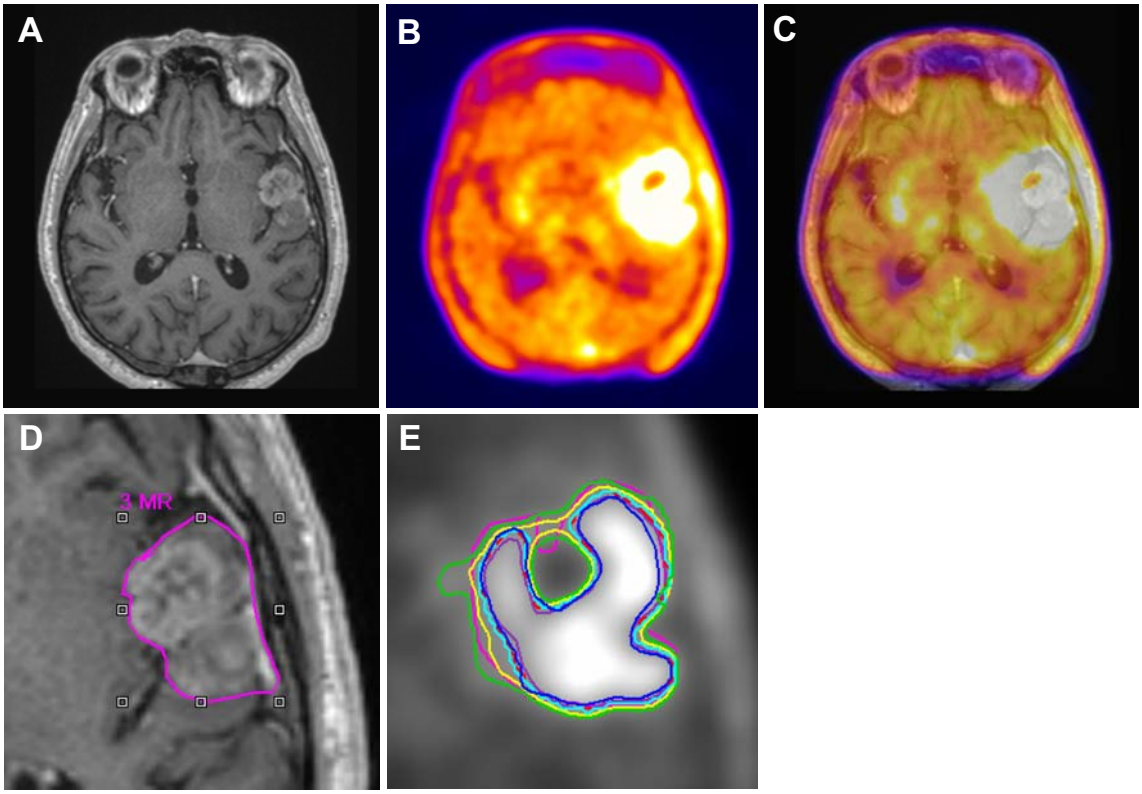

Fig. 4 (**A**) Gadolinium enhanced T1-weighted MRI, (**B**) corresponding ^{18}F-FET PET, and fused PET/MR (**C**) transaxial slices of a clinical study with a glioblastoma showing differences in target-volume definition. Indicated are (**D**) the gross tumor volume (GTV) delineated on MRI (GTV_{MRI}), and (**E**) enhanced details of PET-based GTVs obtained by manual delineation of contours (GTV_{man}; *magenta*), an isocontour of a standardized uptake value (SUV) of 2.5 ($GTV_{2.5}$; *purple*), a fixed threshold of 40% ($GTV_{40\%}$; *green*) and 50% ($GTV_{50\%}$; *cyan*) of the maximum signal intensity, signal-to-background ratio (SBR)-based adaptive thresholding (GTV_{SBR}; *yellow*), gradient find (GTV_{GF}; *blue*), and region growing (GTV_{RG}; *red*) segmentation algorithms. Note that GTV_{MRI} overestimates the tumor extension relative to GTV_{man}

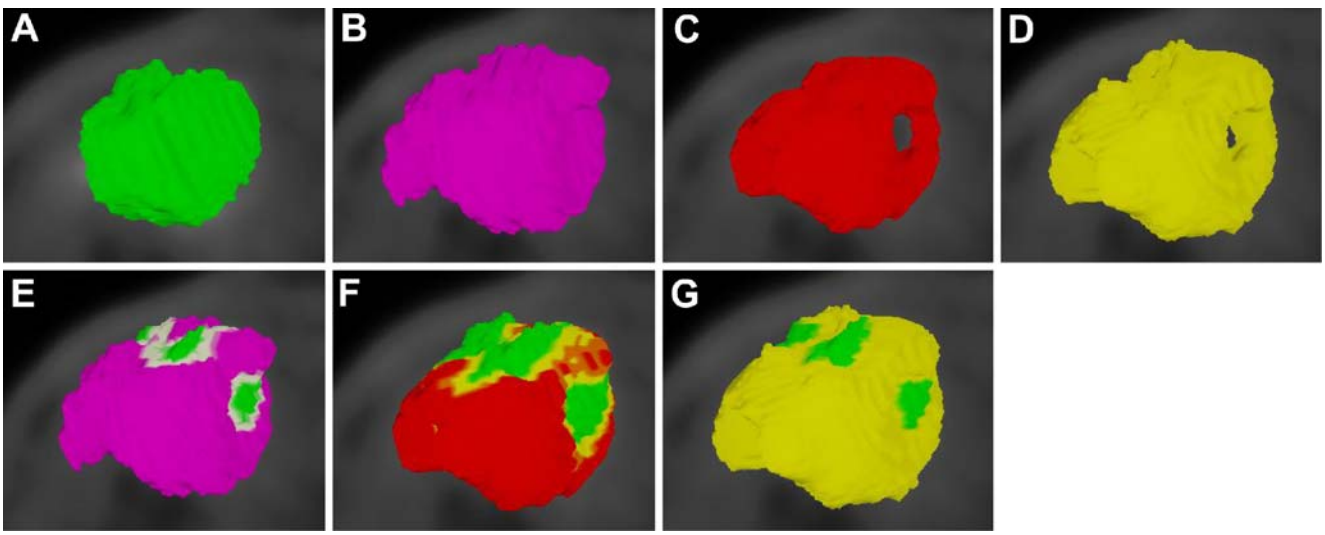

Fig. 5 Three-dimensional volume rendering of the gross tumor volumes (GTVs) assessed using the various segmentation techniques and overlap analysis of the geographic match/mismatch between the defined GTVs. Indicated are (**A**) the GTV delineated on MRI (GTV_{MRI}), and the PET-based GTVs obtained by (**B**) manual delineation of contours (GTV_{man}), (**C**) region growing (GTV_{RG}), (**D**) signal-to-background ratio (SBR)-based adaptive thresholding (GTV_{SBR}). Also shown are the overlaps between GTV_{MRI} relative to GTV_{man} (**E**), GTV_{MRI} relative to GTV_{RG} (**F**), and GTV_{MRI} relative to GTV_{SBR} (**G**). Note that for this particular tumor, GTV_{man} practically comprised approximately 95% of GTV_{MRI}

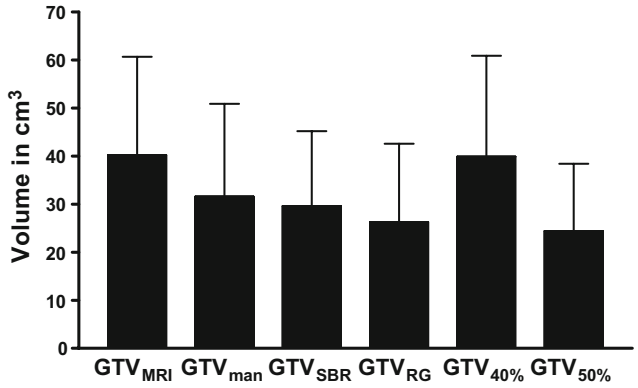

Fig. 6 Comparison of mean tumor volumes for 18 patients and in only 19 lesions where MRI, manual delineation, thresholding using 40% and 50% of the maximum intensity, as well as RG and SBR techniques were able to adequately delineate the tumor volume. *Error bars* indicate SD on the mean. Results are shown for the gross tumor volume (GTV) delineated on MRI (GTV_{MRI}) and PET-based GTVs obtained by manual delineation of contours (GTV_{man}), an isocontour obtained using a fixed threshold of 40% ($GTV_{40\%}$) and 50% ($GTV_{50\%}$) of the maximum signal intensity, signal-to-background ratio (SBR)-based adaptive thresholding (GTV_{SBR}), and region growing (GTV_{RG}) segmentation algorithms

technique validated thoroughly using histologic data [39] and was hypothesized to be the most accurate one for high SBR levels [23]. ^{18}F-FET and ^{11}C-MET PET tracers have been shown to be in a close correlation when imaging human brain tumors [40]. A thorough assessment of the impact of ^{18}F-FET PET on the delineation of GTV is lacking compared to ^{11}C-MET PET. A prospective study using ^{18}F-FET PET and MRI in patients with suspected cerebral glioma concluded that the combined use of MRI and ^{18}F-FET PET was clearly superior to that of MRI alone for the noninvasive distinction of tumor tissue and peritumoral brain tissue [6]. The combined MRI–FET PET approach was able to image the true extent of cerebral gliomas with a high sensitivity and specificity (93% and 94%, respectively). On the other hand, MRI alone had a low specificity (only 53%). A tumour-to-normal brain threshold of 1.6 for ^{18}F-FET uptake was found the best ratio to detect the extent of gliomas and to distinguish between malignant and benign lesions in the brain [6, 33]. Grosu et al. were the first to show a survival benefit for patients reirradiated for recurrent high-grade gliomas using ^{11}C-MET PET or 3–123I-iodo-alpha-methyl-L-tyrosine SPECT/CT/MRI image fusion in the treatment planning, in comparison to patients treated based on MRI/CT alone [36]. In studies for target definition using ^{11}C-MET PET, a threshold value of 1.7 for the tumour/normal brain index was used [37, 38]. In addition, it was demonstrated that the fusion between MRI and ^{11}C-MET PET results in significantly higher specificity and accuracy in GTV delineation compared to MRI alone. Grosu et al. compared ^{11}C-MET PET and MRI in resected high-grade gliomas using image fusion for radiation therapy treatment planning and showed that the majority of patients had a poor correlation of the morphological and the biological tumor volume [37]. The region of ^{11}C-MET uptake was larger than that of gadolinium-enhanced MRI in 31 of 39 cases (79%), and in a majority of patients, the gadolinium-enhancement area extended beyond the MET enhancement. A retrospective study by Mahasittiwat et al. [38] confirmed these results and found a significantly greater survival and distant control rate in patients where the ^{11}C-MET uptake did not extend outside the clinical target volume. It has also been reported that MR spectroscopy (MRS) can detect residual cancer after surgery with a higher sensitivity and specificity compared to MRI [41].

The development of medical image segmentation and other image analysis techniques have been very rapid and

Table 3 Summary of gross tumour volumes delineated using the different methods and overlap fractions (OFs) between various segmentation tools

Segmentation Method	Mean volume in cc (95% CI)	Mean OF_{SBR} (95% CI)	Mean OF_{MRI} (95% CI)	*P* value	Mean OF_{PET} (95% CI)	*P* value
GTV_{MRI}	40.24 (30.37–50.11)	–	–	–	–	–
GTV_{man}	31.62 (20.30–40.95)	0.77 (0.66–0.88)	0.45 (0.33–0.56)	NS	0.61 (0.52–0.71)	< 0.001
GTV_{SBR}	29.55 (22.02–37.08)	–	0.44 (0.33–0.55)	–	0.62 (0.50–0.74)	–
$GTV_{40\%}$	39.90 (29.77–50.02)	0.99 (0.97–1.00)	0.54 (0.42–0.66)	< 0.001	0.57 (0.46–0.67)	< 0.001
$GTV_{50\%}$	24.37 (19.62–31.11)	0.73 (0.64–0.82)	0.36 (0.26–0.46)	< 0.001	0.67 (0.56–0.79)	< 0.001
GTV_{RG}	26.35 (18.50–34.19)	0.74 (0.65–0.82)	0.37 (0.28–0.47)	< 0.001	0.65 (0.53–0.78)	< 0.001
GTV_{GF}	–	0.49 (0.33–0.65)	0.21 (0.11–0.31)	NS	0.45 (0.25–0.66)	< 0.01
$GTV_{2.5}$	–	0.29 (0.16–0.41)	0.14 (0.06–0.21)	NS	0.67 (0.49–0.86)	< 0.01

The mean volumes are for 18 patients and only in 19 lesions where MRI, manual delineation, thresholding using 40% and 50% of the maximum intensity, as well as RG and SBR techniques were able to adequately delineate the tumour volume (GF and SUV 2.5 were excluded in this analysis). The *p* values are for OFs relative to OF of SBR (OF_{SBR}) obtained by linear regression analysis. OF_{SBR} is a comparison of OF within PET defined volumes hence no estimate for MRI volume. The *p* values are reported for each segmentation technique relative to GTV_{SBR}

exciting, and there is every reason to believe the field will move forward more rapidly in the near future with the advent of better computing power and the unlimited imagination of active researchers in the field. Our work aimed at assessing various strategies for delineation of GTVs for high-grade gliomas. A limited number of publications reported on the comparative assessment of various image segmentation techniques for GTV delineation [21, 23]. Automated segmentation techniques are important for defining the target volume thus allowing alleviating the difficult time-consuming manual procedures. Despite the remarkable progress that automated image segmentation has made during the last few years, performance validation in a clinical setting remains the most challenging issue [15]. Evaluation and clinical validation of image segmentation techniques and data quantification algorithms is inherently difficult and sometimes unconvincing particularly when applied to image-guided therapy [27]. A survey of different methods proposed for evaluation of image segmentation algorithms including the criteria for choosing figures of merit is given elsewhere [42]. However, most of these techniques require the availability of reference data where the ground truth is known. Further validation within the framework of a prospective study using in vivo macroscopic surgical specimen of oncologic patients allowing thorough qualitative and quantitative comparison of image segmentation results with the surgical specimen considered as gold standard is clearly needed but remains difficult in the case of brain tumors.

Conclusion

Besides the role of ^{18}F-FET PET/CT in the delineation of treatment volumes for radiation therapy treatment planning, the technique had a major impact on further clinical management of patients with high-grade gliomas. Eighteen clinical image volumes were used to portray the contrasting results obtained when using various PET-guided strategies to delineate GTVs relative to MRI-guided delineation. Overall, the majority of GTVs defined on PET-based techniques were usually smaller than GTV_{MRI} (67% of cases). Yet, PET detected frequently tumors that are not visible on MRI and added substantially tumor extension outside the GTV_{MRI} in six patients (33% of cases). The choice of the most appropriate PET-based segmentation algorithm is crucial, since it impacts both the volume and shape of the ensuing GTV. $SUV_{2.5}$ and GF segmentation techniques performed poorly and should not be used for GTV delineation. The SBR algorithm, as the only technique validated through a histologic study, can be used with confidence as it has some practical advantages particularly for adapting the threshold to the patient-specific SBR and for limiting intra- and inter-observer dependence and variability. With adequate delineation, PET may add considerably to conventional MRI-guided GTV delineation.

Acknowledgments This work was supported by the Swiss National Science Foundation under grant No. 3152A0-102143, the Indo Swiss Bilateral Research Initiative (ISBRI) supported by the Swiss State Secretariat for Education and Research under grant No. AP24, and the foundation Cellex International. This paper is dedicated to the memory of Prof. Bruce Hasegawa (Department of Radiology, UCSF), a brilliant scientist and true friend who sadly passed away last summer.

References

1. Omuro AM, Delattre JY. Editorial: what is new in the treatment of gliomas? Curr Opin Neurol 2007;20:704–7.
2. DeAngelis LM. Brain tumors. N Engl J Med 2001;344:114–23.
3. Popperl G, Tatsch K, Kreth FW, Tonn JC. Brain tumors. Recent Results Cancer Res 2008;170:33–47.
4. Chamberlain MC, Murovic JA, Levin VA. Absence of contrast enhancement on CT brain scans of patients with supratentorial malignant gliomas. Neurology 1988;38:1371–4.
5. Rachinger W, Goetz C, Popperl G, et al. Positron emission tomography with *O*-(2-[18F]fluoroethyl)-l-tyrosine versus magnetic resonance imaging in the diagnosis of recurrent gliomas. Neurosurgery 2005;57:505–11.
6. Pauleit D, Floeth F, Hamacher K, et al. *O*-(2-[18F]fluoroethyl)-L-tyrosine PET combined with MRI improves the diagnostic assessment of cerebral gliomas. Brain 2005;128:678–87.
7. Chen W. Clinical applications of PET in brain tumors. J Nucl Med 2007;48:1468–81.
8. Jager PL, Vaalburg W, Pruim J, de Vries EG, Langen KJ, Piers DA. Radiolabeled amino acids: basic aspects and clinical applications in oncology. J Nucl Med 2001;42:432–45.
9. Heiss P, Mayer S, Herz M, Wester HJ, Schwaiger M, Senekowitsch-Schmidtke R. Investigation of transport mechanism and uptake kinetics of *O*-(2-[18F]fluoroethyl)-L-tyrosine in vitro and in vivo. J Nucl Med 1999;40:1367–73.
10. Spaeth N, Wyss MT, Weber B, et al. Uptake of 18F-fluorocholine, 18F-fluoroethyl-L-tyrosine, and 18F-FDG in acute cerebral radiation injury in the rat: implications for separation of radiation necrosis from tumor recurrence. J Nucl Med 2004;45:1931–8.
11. Popperl G, Goldbrunner R, Gildehaus FJ, et al. *O*-(2-[18F] fluoroethyl)-L-tyrosine PET for monitoring the effects of convection-enhanced delivery of paclitaxel in patients with recurrent glioblastoma. Eur J Nucl Med Mol Imaging 2005;32:1018–25.
12. Mehrkens JH, Popperl G, Rachinger W, et al. The positive predictive value of *O*-(2-[(18)F]fluoroethyl)-L-tyrosine (FET) PET in the diagnosis of a glioma recurrence after multimodal treatment. J Neurooncol 2008;88:27–35.
13. Pauleit D, Floeth F, Tellmann L, et al. Comparison of *O*-(2–18F-fluoroethyl)-L-tyrosine PET and 3-123I-iodo-alpha-methyl-L-tyrosine SPECT in brain tumors. J Nucl Med 2004;45:374–81.
14. Gregoire V, Haustermans K, Geets X, Roels S, Lonneux M. PET-based treatment planning in radiotherapy: A new standard? J Nucl Med 2007;48:68S–77S.
15. Boudraa A, Zaidi H. Image segmentation techniques in nuclear medicine imaging. In: Zaidi H, editor. Quantitative analysis of nuclear medicine images. New York: Springer; 2006. p. 308–57.
16. van Baardwijk A, Baumert BG, Bosmans G, et al. The current status of FDG-PET in tumour volume definition in radiotherapy treatment planning. Cancer Treat Rev 2006;32:245–60.

17. Erdi Y, Mawlawi O, Larson S, et al. Segmentation of lung lesion volume by adaptive positron emission tomography image thresholding. radioimmunodetection and radioimmunotherapy of cancer, Princeton, New Yersey, 1997:2505–2509.
18. Daisne JF, Sibomana M, Bol A, Doumont T, Lonneux M, Gregoire V. Tri-dimensional automatic segmentation of PET volumes based on measured source-to-background ratios: influence of reconstruction algorithms. Radiother Oncol 2003;69:247–50.
19. Ciernik IF, Dizendorf E, Baumert BG, et al. Radiation treatment planning with an integrated positron emission and computer tomography (PET/CT): a feasibility study. Int J Radiat Oncol Biol Phys 2003;57:853–63.
20. Yaremko B, Riauka T, Robinson D, et al. Thresholding in PET images of static and moving targets. Phys Med Biol 2005;50:5969–82.
21. Nestle U, Kremp S, Schaefer-Schuler A, et al. Comparison of different methods for delineation of 18F-FDG PET-positive tissue for target volume definition in radiotherapy of patients with non-Small cell lung cancer. J Nucl Med 2005;46:1342–8.
22. Drever L, Roa W, McEwan A, Robinson D. Iterative threshold segmentation for PET target volume delineation. Med Phys 2007;34:1253–65.
23. Schinagl DA, Vogel WV, Hoffmann AL, van Dalen JA, Oyen WJ, Kaanders JH. Comparison of five segmentation tools for 18F-fluoro-deoxy-glucose-positron emission tomography-based target volume definition in head and neck cancer. Int J Radiat Oncol Biol Phys 2007;69:1282–9.
24. Hatt M, Lamare F, Boussion N, et al. Fuzzy hidden Markov chains segmentation for volume determination and quantitation in PET. Phys Med Biol 2007;52:3467–91.
25. Montgomery D, Amira A, Zaidi H. Fully automated segmentation of oncological PET volumes using a combined multiscale and statistical model. Med Phys 2007;34:722–36.
26. Hong R, Halama J, Bova D, Sethi A, Emami B. Correlation of PET standard uptake value and CT window-level thresholds for target delineation in CT-based radiation treatment planning. Int J Radiat Oncol Biol Phys 2007;67:720–6.
27. Jannin P, Fitzpatrick JM, Hawkes DJ, Pennec X, Shahidi R, Vannier MW. Validation of medical image processing in image-guided therapy. IEEE Trans Med Imaging 2002;21:1445–9.
28. Pauleit D, Floeth F, Herzog H, et al. Whole-body distribution and dosimetry of *O*-(2-[18F]fluoroethyl)-L-tyrosine. Eur J Nucl Med Mol Imaging 2003;30:519–24.
29. Graves EE, Quon A, Loo BW Jr. RT_Image: an open-source tool for investigating PET in radiation oncology. Technol Cancer Res Treat 2007;6:111–21.
30. Jentzen W, Freudenberg L, Eising EG, Heinze M, Brandau W, Bockisch A. Segmentation of PET volumes by iterative image thresholding. J Nucl Med 2007;48:108–14.
31. Basu S, Zaidi H, Houseni M, et al. Novel quantitative techniques for assessing regional and global function and structure based on modern imaging modalities: Implications for normal variation, aging and diseased states. Sem Nucl Med 2007;37:223–39.
32. Plotkin M, Gneveckow U, Meier-Hauff K, et al. 18F-FET PET for planning of thermotherapy using magnetic nanoparticles in recurrent glioblastoma. Int J Hyperthermia 2006;22:319–25.
33. Floeth FW, Pauleit D, Sabel M, et al. 18F-FET PET differentiation of ring-enhancing brain lesions. J Nucl Med 2006;47:776–82.
34. Langen KJ, Floeth FW, Stoffels G, Hamacher K, Coenen HH, Pauleit D. Improved diagnostics of cerebral gliomas using FET PET. Z Med Phys 2007;17:237–41.
35. Mosskin M, von Holst H, Bergstrom M, et al. Positron emission tomography with 11C-methionine and computed tomography of intracranial tumours compared with histopathologic examination of multiple biopsies. Acta Radiol 1987;28:673–81.
36. Grosu AL, Weber WA, Franz M, et al. Reirradiation of recurrent high-grade gliomas using amino acid PET (SPECT)/CT/MRI image fusion to determine gross tumor volume for stereotactic fractionated radiotherapy. Int J Radiat Oncol Biol Phys 2005;63:511–9.
37. Grosu AL, Weber WA, Riedel E, et al. L-(methyl-11C) methionine positron emission tomography for target delineation in resected high-grade gliomas before radiotherapy. Int J Radiat Oncol Biol Phys 2005;63:64–74.
38. Mahasittiwat P, Mizoe JE, Hasegawa A, et al. *l*-[METHYL-(11)C] methionine positron emission tomography for target delineation in malignant gliomas: impact on results of carbon ion radiotherapy. Int J Radiat Oncol Biol Phys 2008;70:515–22.
39. Daisne JF, Dupers T, Weygand B, et al. Tumor volume in pharyngolaryngeal squamous cell carcinoma: comparison at CT, MR imaging, and FDG PET and validation with surgical specimen. Radiology 2004;233:93–100.
40. Weber WA, Wester HJ, Grosu AL, et al. *O*-(2-[18F]fluoroethyl)-L-tyrosine and L-[methyl-11C]methionine uptake in brain tumours: initial results of a comparative study. Eur J Nucl Med 2000;27:542–9.
41. Pirzkall A, Li X, Oh J, et al. 3D MRSI for resected high-grade gliomas before RT: tumor extent according to metabolic activity in relation to MRI. Int J Radiat Oncol Biol Phys 2004;59:126–37.
42. Zhang YJ. A survey on evaluation methods for image segmentation. Patt Recogn Letters 1996;29:1335–46.